Single-particle states and parity doublets in odd-Z ^{221}Ac and ^{225}Pa from α-decay spectroscopy

E. Parr,[1,2] J. F. Smith,[1,2] P. T. Greenlees,[3] P. A. Butler,[4] K. Auranen,[3] R. Chapman,[1,2] D. M. Cox,[3,*] D. M. Cullen,[5] L. P. Gaffney,[1,2,†] T. Grahn,[3] E. T. Gregor,[1,2] L. Grocutt,[1,2] A. Herzáň,[3,6] R.-D. Herzberg,[4] D. Hodge,[5] U. Jakobsson,[3] R. Julin,[3] S. Juutinen,[3] J. M. Keatings,[1,2] J. Konki,[3] M. Leino,[3] P. P. McKee,[1,2] C. McPeake,[4] D. Mengoni,[7] A. K. Mistry,[4,‡] B. S. Nara Singh,[5,§] G. G. O'Neill,[4] J. Pakarinen,[3] P. Papadakis,[3,‖] J. Partanen,[3,¶] P. Peura,[3] P. Rahkila,[3] P. Ruotsalainen,[3] M. Sandzelius,[3] J. Sarén,[3] M. Scheck,[1,2] C. Scholey,[3] M. Siciliano,[3,7,#] M. Smolen,[1,2] J. Sorri,[3,**] P. Spagnoletti,[1,2] K. M. Spohr,[1,2,††] S. Stolze,[3] M. J. Taylor,[5,‡‡] and J. Uusitalo[3]

[1]*School of Computing, Engineering, and Physical Sciences, University of the West of Scotland, Paisley PA1 2BE, United Kingdom*
[2]*Scottish Universities Physics Alliance, Glasgow, United Kingdom*
[3]*University of Jyvaskyla, Department of Physics, P.O. Box 35, FI-40014 University of Jyvaskyla, Finland*
[4]*Oliver Lodge Laboratory, University of Liverpool, Liverpool L69 7ZE, United Kingdom*
[5]*School of Physics and Astronomy, Schuster Building, University of Manchester, Manchester M13 9PL, United Kingdom*
[6]*Institute of Physics, Slovak Academy of Sciences, SK-84511 Bratislava, Slovakia*
[7]*Dipartimento di Fisica e Astronomia dell' Università and INFN Sezione di Padova, Padova, Italy*

(Received 7 October 2021; accepted 2 February 2022; published 2 March 2022)

Low-lying states in the odd-Z isotopes $^{221}_{89}\mathrm{Ac}_{132}$ and $^{225}_{91}\mathrm{Pa}_{134}$ have been studied using α-particle and $\alpha\gamma$-coincidence spectroscopy in the $^{225}\mathrm{Pa} \rightarrow {}^{221}\mathrm{Ac} \rightarrow {}^{217}\mathrm{Fr}$ decay chain. Ground-state spin and parity assignments of $I^{\pi} = 5/2^{-}$ are proposed for both ^{221}Ac and ^{225}Pa, with the odd proton occupying the $\Omega = 5/2$ orbital of the quadrupole-octupole deformed shell model in both nuclei. In ^{221}Ac, excited states in the bands based on the $\Omega = 5/2$ and $\Omega = 3/2$ orbitals have been identified, including proposed parity-doublet states. The results suggest that reflection-asymmetric deformation of the ground state persists in the odd-A members of the isotope chains down to $N = 132$ for Ac and $N = 134$ for Pa, before reaching the transitional region at $N = 130$.

DOI: 10.1103/PhysRevC.105.034303

I. INTRODUCTION

The phenomenon of octupole correlations in atomic nuclei has been a subject of considerable interest for the past few decades [1–3]. In the presence of strong octupole correlations, static reflection-asymmetric deformations of the nucleus can be induced. The strongest octupole correlations, and hence the most pronounced reflection-asymmetric octupole shapes, are found in nuclei in the light-actinide region, centered around $N = 136$ and $Z = 88$. Shell-model calculations of single-particle orbitals in this region, therefore, need to include both quadrupole and octupole deformation of the nuclear potential [4–6]. Calculations of this nature indicate that the inclusion of an asymmetric deformation component results in significant changes to single-particle energies and orderings for proton and neutron orbitals. Experimentally, it is therefore of great interest to study the properties of low-lying states in the light-actinide region, which can be compared to the predictions of shell-model calculations with and without an octupole-deformed component. Comparison of experimentally assigned ground-state spins and parities with expectations from different calculations, based on occupancies of the lowest-lying neutron (odd-N) or proton (odd-Z) orbitals, can help to elucidate the extent of nuclei which possess ground-state octupole deformation. This type of analysis was carried out for the odd-A light-actinide nuclei almost 35 years ago by Sheline, as described in Ref. [7]. That work

*Present address: Department of Physics, Lund University, 22100 Lund, Sweden.
†Present address: Oliver Lodge Laboratory, University of Liverpool, Liverpool L69 7ZE, United Kingdom.
‡Present address: Institut fur Kernphysik, Technische Universität Darmstadt, Darmstadt, Germany.
§Present address: School of Computing, Engineering, and Physical Sciences, University of the West of Scotland, Paisley PA1 2BE, United Kingdom.
‖Present address: Nuclear Physics Group, STFC Daresbury Laboratory, Daresbury, Warrington WA4 4AD, United Kingdom.
¶Deceased.
#Present address: Physics Division, Argonne National Laboratory, Argonne, Illinois 60439, USA.
**Present address: Radiation and Nuclear Safety Authority STUK, Laippatie 4, Helsinki, Finland.
††Present address: Extreme Light Infrastructure (ELI-NP) and Horia Hulubei National Institute for R&D in Physics and Nuclear Engineering (IFIN-HH), Str. Reactorului No. 30, 077125 Bucharest-Măgurele, Romania.
‡‡Present address: Division of Cancer Sciences, School of Medical Sciences, The University of Manchester, Manchester M13 9PL, United Kingdom.

tentatively established the extent of the region of ground-state octupole deformation in the light actinides. Although a significant amount of new experimental data has been obtained since the work of Sheline, there remains a paucity of data to define the region at the lower-N boundary, close to $N = 130$, and at the higher-Z boundary, around $Z = 91$ (Pa) and $Z = 92$ (U). Interest in determining the extent of this region has also been reignited recently, with theoretical calculations predicting ground-state octupole deformations to persist in even-even nuclei up to ^{226}Fm ($N = 126$, $Z = 100$) [8].

A valuable experimental method in the study of low-lying states in the light-actinide region is α-decay spectroscopy. Low-lying excited states are often populated by the α decay. In addition to the energies of the states populated, derived from differences in α-decay Q values, the spectrum of low-lying excited states (level scheme) may be inferred from the detection of coincident γ rays and internal conversion electrons. This $\alpha\gamma$ (or αe) method often enables the multipolarities of transitions to be determined, which then provide information about the spins and parities (I^π) of the initial and final states involved in the transition. Hindrance factors (HF) of α decay can also be derived; the hindrance factor is the ratio of the experimentally-determined partial half-life of a decay to that calculated by a simple model where the preformed α particle lies in the potential of the daughter nucleus. Values of HF indicate the similarity of the underlying structures of the initial and final states in an α-decay transition. This helps us to interpret not only the I^π assignment and configuration of the state that is populated, but also those of the decaying state. This latter consideration has previously been somewhat overlooked and can enable the configurations of α-decaying states to be interpreted along isotope and isotone chains, often reaching otherwise experimentally challenging nuclei.

Here, the odd-Z light-actinide nuclei ^{221}Ac ($Z = 89$) and ^{225}Pa ($Z = 91$) have been studied using α-decay and $\alpha\gamma/\alpha e$-coincidence spectroscopy. The α-decaying nuclei were produced in heavy-ion fusion-evaporation reactions or were themselves produced in α decay. New results concerning the low-lying states involved in the α decay, including spin and parity assignments, have been compared to theoretical predictions and regional systematics to help us understand the strength of octupole correlations in these nuclei.

II. PREVIOUS RESULTS

A. ^{221}Ac → ^{217}Fr α decay

The ground-state spin and parity of ^{221}Ac have previously been tentatively assigned to be $I^\pi = (3/2^-)$; this assignment was made following an in-beam γ-ray spectroscopy study in which ^{221}Ac was produced by the ^{209}Bi(^{14}C, $2n$)^{221}Ac reaction [9]. The α decay of ^{221}Ac was previously studied several times in Refs. [10–14], with consistent results reported for α-particle energies and branching ratios for up to four α decays. Energies of excited states populated in ^{217}Fr following the α decays of ^{221}Ac, with [E_α (keV), BR$_\alpha$ (%)], were determined to be 210(20) [7440(15), 20(5)], 270(20) [7375(10), 10(5)], and 485(15) keV [7170(10), ≈2]. The excitation energies were calculated from α-particle energy differences [11], assuming the [7645(10), 70(10)] α decay populates the ground state. The ground state of ^{217}Fr has been determined to have $I^\pi = 9/2^-$ from the identification of a dominant, unhindered α decay from ^{217}Fr to the ground state of the spherical nucleus ^{213}At [11]. No spin and parity assignments were made in Refs. [10–14] for the excited states in ^{217}Fr populated by ^{221}Ac α decay and the states were not observed in prompt γ-ray spectroscopy [15].

B. ^{225}Pa → ^{221}Ac α decay

No excited states have been identified in ^{225}Pa and no assignment for the I^π of the α-decaying ground state has previously been made. The α decay of ^{225}Pa has previously been reported in Refs. [10–12,14,16] with up to three decay branches. The α-particle energies and branching ratios measured in the more comprehensive of these studies were [7250(20) keV, 100%] [10], [7245(10) keV, 70(10)%], [7195(10) keV, 30(10)%] [11] and [7261(5) keV, 53(2)%], [7235(5) keV, 30(2)%], [7170(5) keV, 17(1)%] [12]. Some disagreement exists in the detail of the α-decay fine structure following these previous studies. However, the results from Ref. [12] are considered the most authoritative, due to the clean spectra presented. Using these α-particle energies the excited states populated in ^{221}Ac have energies of 26(7) and 92(7) keV, assuming that the 7261-keV α-particle decay populates the ground state. The prompt γ-ray study of ^{221}Ac led to the tentative $I^\pi = (3/2^-)$ ground-state assignment and a scheme of around 30 proposed levels [9]; however, there are no candidates with energies corresponding to those populated following the α decay of ^{225}Pa.

III. EXPERIMENTAL DETAILS

The results presented in this paper are taken from two experiments that were performed at the Accelerator Laboratory of the University of Jyväskylä in Finland. Nuclei were produced via fusion-evaporation reactions using ^{208}Pb targets and beams of ^{18}O (Experiment 1) and ^{20}Ne (Experiment 2). Details of the energies and intensities of beams, as well as target thicknesses and experimental duration, are given in Table 1 of Ref. [17]. The experiments were both performed with the same experimental set up, which is described below. The target was located at the center of the SAGE spectrometer [18], which was used to detect prompt γ rays and internal-conversion electrons; however, data from the SAGE spectrometer are not presented in this paper. Downstream of the target, recoiling evaporation residues were separated from fission fragments and unreacted beam ions using the RITU gas-filled recoil separator [19,20] and were transported to its focal plane. The reaction products were then implanted into one of two double-sided silicon strip detectors (DSSDs) placed side-by-side at the focal plane of RITU. This enabled the detection of both the implantation of the product nuclei as well as any charged particles emitted following their decay, or those from the decay of any nuclei produced in subsequent decays. The DSSDs each consisted of 40 horizontal strips and 60 vertical strips, giving a total of 4800 individual pixels. In

standard operation, a multiwire proportional counter (MWPC) is placed in front (upstream) of the DSSDs; the purpose of the MWPC is to provide energy-loss and time-of-flight information to help distinguish between evaporation residues and scattered beam. However, the MWPC was not used in the experiments described here due to the low energies of the evaporation residues. In the present work, time-of-flight information was extracted from the time between prompt signals in SAGE and the subsequent corresponding (implantation) signal in the DSSDs. Along with the DSSDs a suite of supplementary detectors at the focal plane constitute the GREAT spectrometer [21]. This is used to detect radiation emitted following the decays of implanted nuclei, or those in the subsequent decay chain. For the detection of x rays and γ rays emitted from implanted nuclei, three high-purity germanium (HPGe) clover detectors were placed around the DSSDs. Relative to the central ion trajectory, the centers of the clover detectors had polar coordinates (θ, ϕ) of $(90^\circ, 0^\circ)$, $(90^\circ, 90^\circ)$, and $(90^\circ, 270^\circ)$, where $\phi = 0^\circ$ is defined to be vertically upwards.

IV. DATA ANALYSES

Data were acquired using the triggerless Total Data Readout (TDR) system [22] and were analyzed using the GRAIN software package [23], which was specifically developed for use with TDR data. Energy calibration of the DSSD channels was carried out using known α-particle energies emitted from implanted evaporation residues, or those produced in their decay chains. The α decays from ^{210}Po [$E_\alpha = 5304.33(7)$ keV], ^{220}Ra [$E_\alpha = 7456(5)$ keV], ^{219}Ra [$E_\alpha = 7679(3)$ keV], ^{222}Th [$E_\alpha = 7986(3)$ and 7604(3) keV], ^{213}Rn [$E_\alpha = 8090(3)$ keV], and ^{221}Th [$E_\alpha = 8469(4)$, 8144(4), and 7728(4) keV] were used for data from Experiment 1. For data from Experiment 2, the same α-particle energies were used, with the exception of those from ^{220}Ra and ^{219}Ra. The α-particle energies used are weighted means taken from Ref. [24], which reviewed all previously published results. The absolute efficiency for the detection of γ rays in the focal-plane HPGe clover detectors was determined from the intensities of α particles from decays which populated excited states measured in the DSSDs compared with those in coincidence with γ rays from the subsequent internal transitions.

A. α-decay selection

The $^{225}\text{Pa} \rightarrow {}^{221}\text{Ac} \rightarrow {}^{217}\text{Fr} \rightarrow {}^{213}\text{At} \rightarrow {}^{209}\text{Bi}$ α-decay chain is shown schematically in Fig. 1; the data are taken from Refs. [12,25–27]. The α decays of the two isotopes studied here were selected by identifying chains of three or four consecutive signals in a single DSSD pixel. These corresponded to the implant of an evaporation residue at time t_0, followed by the subsequent α decays, α_1, α_2, and α_3, at times t_1, t_2, and t_3, respectively. In the analysis, the energies of α_2 or α_3 often corresponded to an energy sum between two successive α decays in a chain. This was due to the very short half-lives of $N = 128$ nuclei in the region ($T_{1/2} < 300$ ns), and the shaping time of the DSSD energy amplifiers, which was set to be 500 ns. A detailed description of α-decay sum-energy spectroscopy is given

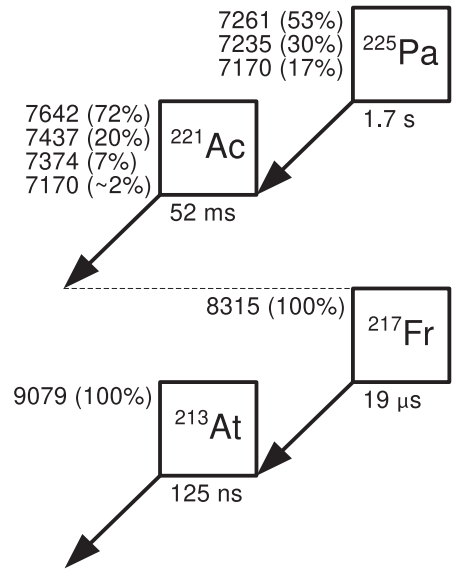

FIG. 1. Schematic representation of the $^{225}\text{Pa} \rightarrow {}^{221}\text{Ac} \rightarrow {}^{217}\text{Fr} \rightarrow {}^{213}\text{At} \rightarrow {}^{209}\text{Bi}$ α-decay chain; data taken from Refs. [12,25–27]. The figure gives α-particle energies, in keV, and branching ratios of the decays, as well as the half-lives of the α-decaying ground states.

in Ref. [17]. In assigning signals as decays, as opposed to reaction-product implantations, the correlation between the energy recorded in the DSSDs (E_{DSSD}) and the time of flight between any signal in SAGE and signals in the DSSDs (t_{TOF}) was used. Two-dimensional gates on plots of these quantities were used to veto signals from being assigned as decays, assuming them therefore to be reaction-product implantations. These gates were centered on (t_{TOF}, E_{DSSD}) coordinates of (2.0 μs, 2.0 MeV) for Experiment 1 and (1.4 μs, 4.4 MeV) for Experiment 2.

1. $^{221}\text{Ac} \rightarrow {}^{217}\text{Fr}$

Data from both Experiments 1 and 2 were used in the study of the α decay from ^{221}Ac. For the data from Experiment 1, α-decay chains were identified whereby α_1 corresponded to the decay of ^{221}Ac ($T_{1/2} = 52$ ms) and α_2 to that of the sum energy between the decays of ^{217}Fr ($T_{1/2} = 19$ μs) and ^{213}At ($T_{1/2} = 125$ ns). Figure 2(a) shows the energy of α_1 plotted against the energy of α_2. Conditions were set for times $(t_1 - t_0)$ from 25 to 364 ms and $(t_2 - t_1)$ from 0 to 133 μs, and for the energy of α_2 from 16.86 to 17.43 MeV. The lower limit on $(t_1 - t_0)$ was set to remove a large background from the $^{222}\text{Th}(T_{1/2} = 2.8\text{ ms}) \rightarrow {}^{218}\text{Ra}(T_{1/2} = 25\ \mu\text{s}) \rightarrow {}^{214}\text{Rn}(T_{1/2} = 270\text{ ns})$ α-decay chain. The lower limit on the energy of α_2 was set to remove background from the $^{220}\text{Ra}(T_{1/2} = 18\text{ ms}) \rightarrow {}^{216}\text{Rn}(T_{1/2} = 45\ \mu\text{s}) \rightarrow {}^{212}\text{Po}(T_{1/2} = 299\text{ ns})$ α-decay chain, where α_2 has a maximum α-particle sum energy of $E_\alpha(^{216}\text{Rn}) + E_\alpha(^{212}\text{Po}) = 16.83$ MeV. The maximum α-particle sum energy of $E_\alpha(^{217}\text{Fr}) + E_\alpha(^{213}\text{At})$ is 17.39 MeV, which determined the upper limit on the α_2 energy. The reduction in background provided by $\alpha\gamma$-coincidence analysis allowed for more liberal conditions of 3.2 to 364 ms

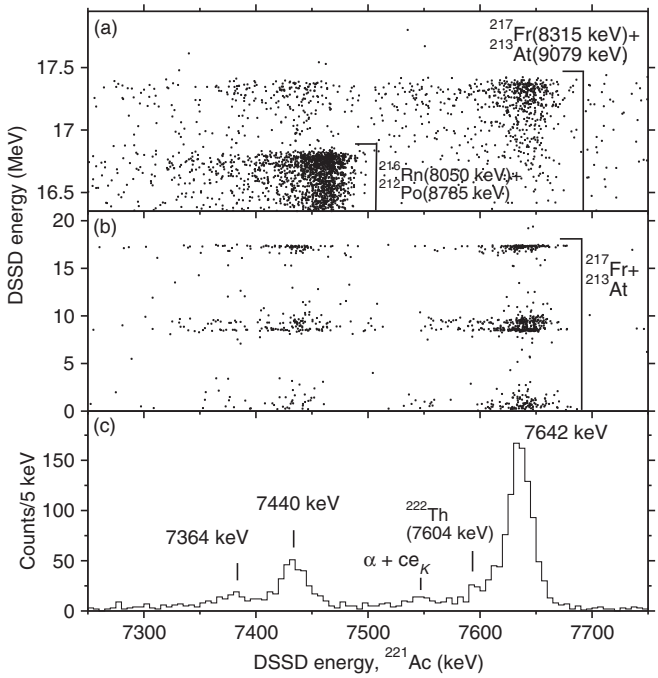

FIG. 2. Spectra showing the α decay of ^{221}Ac. The top two panels show the energies from the ^{221}Ac α decays against those of the subsequent α-particle sums from ^{217}Fr + ^{213}At; taken from Experiments 1 (a) and 2 (b). The bottom panel (c) shows the combined results from both experiments for ^{221}Ac energies. The conditions used to create the spectra are described in the text.

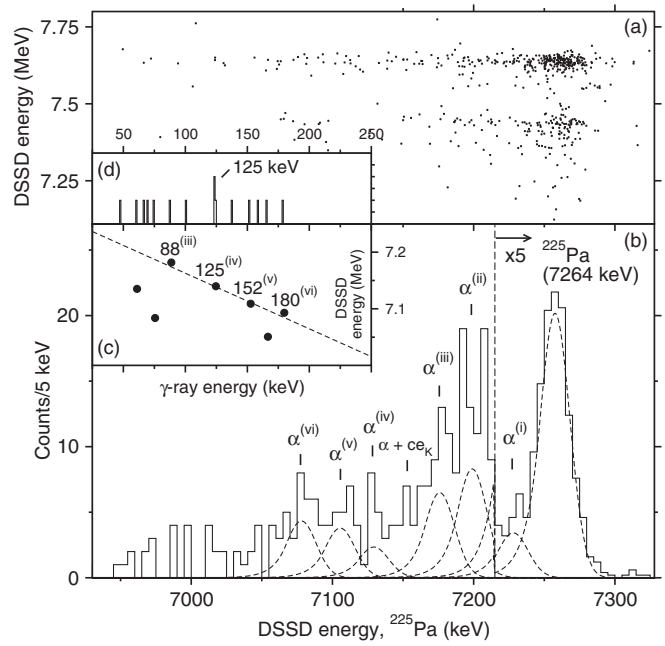

FIG. 3. Spectra from the α decay of ^{225}Pa taken from Experiment 2. The figure shows the energies from the α decay of ^{225}Pa plotted against those from the subsequent ^{221}Ac, panel (a), along with just those selected from ^{225}Pa, panel (b). Panel (c) shows the energies of coincident γ rays and α particles from the decay of ^{225}Pa, with the total Q value for the decay, Q_T, represented as a dashed diagonal line. Panel (d) shows the total projection of γ-ray energies. Energies of α particles and γ rays from corresponding decays are labeled (i)–(vi), which are also detailed in Table I and represented in Fig. 5. The fitted functions for each of the seven α-particle energy peaks are shown as dashed lines on the spectrum.

for $(t_1 - t_0)$ and 0 to 17.43 MeV for the energy of α_2 to be set to obtain these spectra.

For data from Experiment 2, α-decay chains were identified whereby α_1 corresponded to the decay of ^{225}Pa ($T_{1/2}$ = 1.7 s), α_2 to that of ^{221}Ac ($T_{1/2}$ = 52 ms), and α_3 that of the ^{217}Fr + ^{213}At α-particle sum. Energies of α_2 against α_3 in the chains identified are shown in Fig. 2(b). Conditions were set for times $(t_1 - t_0)$ from 28 ms to 8.5 s, $(t_2 - t_1)$ from 2 to 364 ms, and $(t_3 - t_2)$ from 0 to 133 μs. Conditions on energy were set for α_1 from 0 to 7298 keV, with energies 1585 to 6945 keV excluded to prevent falsely correlated recoil energies, and α_3 from 0 to 17.43 MeV. For spectra of $\alpha\gamma$ coincidences no α_3 was required in the chains identified and the condition on the α_1 energy was set across the total 0 to 7298 keV range.

The combined α-particle spectrum of results from Experiments 1 and 2, with the implementation of the time and energy conditions described, is shown in Fig. 2(c).

2. ^{225}Pa → ^{221}Ac

Data from Experiment 2 were used in the study of the α decay of ^{225}Pa. Chains were identified whereby α_1 corresponded to the decay of ^{225}Pa, α_2 to that of ^{221}Ac, and α_3 that of the ^{217}Fr + ^{213}At α-decay sum. Energies of α_1 against α_2 in the chains identified are shown in Fig. 3(a). Conditions were set for times $(t_1 - t_0)$ from 28 ms to 8.5 s, $(t_2 - t_1)$ from 2 to 364 ms, and $(t_3 - t_2)$ from 0 to 133 μs. Conditions on energies were set for α_2 from 7120 to 7680 keV and α_3 from 0 to 17.43 MeV. For spectra of $\alpha\gamma$ coincidences a condition on the energy of α_2 of 0 to 7680 keV was used. The resulting α-particle spectrum, following the implementation of the time and energy conditions described, is shown in Fig. 3(b).

V. RESULTS

Details of the α decays studied in this work are given in Table I. The table gives the energies of the α particles, branching ratios of the decays, spins, parities, and energies of the states populated, the hindrance factors of the decays, and the half-lives of the ground states of ^{221}Ac and ^{225}Pa measured in the present work. The theoretical half-lives used to obtain the hindrance factors were calculated using the spin-independent method prescribed by Preston [28]. In these calculations, nuclear radii of 9.30 (^{217}Fr) and 9.36 fm (^{221}Ac) were used for the theoretical partial half-lives of the α decays from ^{221}Ac and ^{225}Pa, respectively. Additional ground-state half-lives were measured for ^{217}Fr[$T_{1/2}$ = 23(2) μs], and ^{213}At[$T_{1/2}$ = 127(20) ns], which are subsequent members of the α-decay chain.

Table II gives details of γ-ray transitions in the nuclei produced following α decay. The table gives the energies of the transitions, the excitation energies, spins, and parities of the initial and final states, the multipolarities of the transitions,

TABLE I. Details of α decays from ^{221}Ac $\rightarrow$ ^{217}Fr and ^{225}Pa $\rightarrow$ ^{221}Ac. The table gives α-particle energies, E_α (keV), branching ratios, b_α (%), spins and parities, $I^\pi_{\text{pop.}}$, and excitation energies, $E_{\text{pop.}}$ (keV), of states populated, total Q values, given by Q_α+$E_{\text{pop.}}$, Q_T (keV), and hindrance factors, HF. Energies of α particles from ^{225}Pa $\rightarrow$ ^{221}Ac labeled (i)–(vi) correspond to those in Figs. 3 and 5; those shown in square brackets are tentative. Values for the half-lives of the α-decaying states are also given, $T_{1/2}$.

Mother nucleus	E_α	b_α	$I^\pi_{\text{pop.}}$	$E_{\text{pop.}}$	Q_T	HF
^{221}Ac$(5/2^-)$ [$T_{1/2}$ = 45(3) ms]	7642(3)	71(4)	$9/2^-$	0	7783(3)	5.3(5)
	7440(3)	20(2)	$(5/2)^-$	208.7(11)	7785(3)	4.1(5)
	7364(5)	9(2)	$(7/2)^-$	276.0(10)	7776(6)	5.2(12)
^{225}Pa$(5/2^-)$ [$T_{1/2}$ = 1.95(10) s]	7264(3)	61(6)	$5/2^-$	0	7395(3)	2.6(3)
	7234(4)$^{(i)}$	15(4)	$(7/2^-)$	30(5)[a]		8.1(19)
	[7205(8)$^{(ii)}$]	9(3)	$(9/2^-)$	60(8)[a]		11(5)
	7182(8)$^{(iii)}$	5(2)	$(5/2)^+$	88.2(15)	7400(8)	16(7)
	7135(8)$^{(iv)}$	1.8(6)	$(7/2)^+$	124.9(12)	7389(8)	32(11)
	7112(8)$^{(v)}$	3.7(13)	$(5/2^-)$	152.2(15)	7392(8)	12(5)
	7084(8)$^{(vi)}$	4.0(12)	$(7/2^-)$	179.8(15)	7391(8)	9(3)

[a]Energy taken from difference in α-decay Q values.

and the branching ratios from the initial states, where appropriate. Level schemes representing the ^{221}Ac $\rightarrow$ ^{217}Fr and ^{225}Pa $\rightarrow$ ^{221}Ac α decays and the states populated are shown in Figs. 4 and 5, respectively.

A. ^{221}Ac $\rightarrow$ ^{217}Fr α decay

Figures 2(c) and 6 show the α-particle and $\alpha\gamma$-coincidence spectra for the decay of ^{221}Ac, selected as described in Sec. IV A 1. The highest-energy α particle, with 7642 keV, is assumed to be produced by the decay to the ground state in ^{217}Fr. This assumption is made as no γ rays are observed in coincidence with these α particles and no higher-energy α-particle-conversion-electron sum peaks are present. To help to establish the level scheme of states populated in ^{217}Fr following the α decay of ^{221}Ac, a line of total Q value, Q_T = 7783 keV from the 7642-keV α-particle energy, is shown on Fig. 6(a) as a dashed diagonal line. This represents the total energy of the ^{221}Ac α decay, which consists of the α-particle Q value plus the γ-ray energy. It is therefore likely that $\alpha\gamma$ coincidences which appear on this line are produced by α decays which populate a state in ^{217}Fr which then decays directly via the emission of a single γ ray to the ground state. Energies of the α particles identified from decays of ^{221}Ac which populate excited states in ^{217}Fr are also shown as horizontal lines on the $\alpha\gamma$-coincidence spectrum in Fig. 6(a).

It can be seen from the $\alpha\gamma$-coincidence spectrum that the 7440-keV α particles are emitted from decays which populate a 209-keV state in ^{217}Fr, which then decays directly to the ground state via a 209-keV γ ray. Figure 6(b) shows the γ rays in coincidence with the 7440-keV α particle, and as only the 209-keV γ rays are observed a branching ratio of 100% from the 209-keV state to the ground state is assumed.

The γ rays in coincidence with the 7364-keV α particle, or those summed with Auger electrons, are shown in Fig. 6(c). Coincidences between 7364-keV α particles and 276-keV γ rays which lie on the Q_T line suggest that this α decay populates a state with this excitation energy, which then decays

TABLE II. Details of the γ-ray transitions in daughter nuclei following the ^{221}Ac $\rightarrow$ ^{217}Fr and ^{225}Pa $\rightarrow$ ^{221}Ac α decays. The table gives transition energies, E_γ (keV), energies of initial and final states populated, E_i (keV) and E_f (keV), character of the transition, σL, initial and final spins and parities of states populated, I^π_i and I^π_f, and branching ratios of transitions from states, b_γ (%), where relevant.

Nucleus	E_γ	$E_i \rightarrow E_f$	σL	$I^\pi_i \rightarrow I^\pi_f$	b_γ
^{217}Fr	67.2(15)	276.0 $\rightarrow$ 208.7	$M1$	$(7/2)^- \rightarrow (5/2)^-$	67(30)
	208.7(10)	208.7 $\rightarrow$ 0	$E2$	$(5/2)^- \rightarrow 9/2^-$	
	276.0(11)	276.0 $\rightarrow$ 0	$M1$	$(7/2)^- \rightarrow 9/2^-$	33(17)
^{221}Ac	88.2(15)	88.2 $\rightarrow$ 0	$E1$	$(5/2)^+ \rightarrow 5/2^-$	
	124.9(12)	124.9 $\rightarrow$ 0	$E1$	$(7/2)^+ \rightarrow 5/2^-$	
	152.2(15)	152.2 $\rightarrow$ 0		$(5/2^-) \rightarrow 5/2^-$	
	179.8(15)	179.8 $\rightarrow$ 0		$(7/2^-) \rightarrow 5/2^-$	

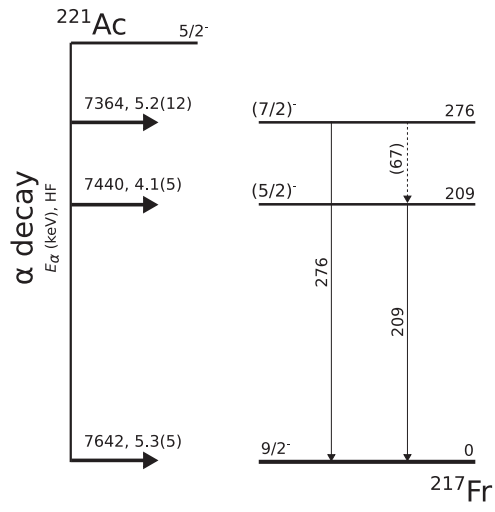

FIG. 4. Level scheme representing the ^{221}Ac $\rightarrow$ ^{217}Fr α decay. The figure shows the α-particle energies and hindrance factors of each decay, as well as the I^π and energy of each state and the energies of transitions. All energies are given in keV.

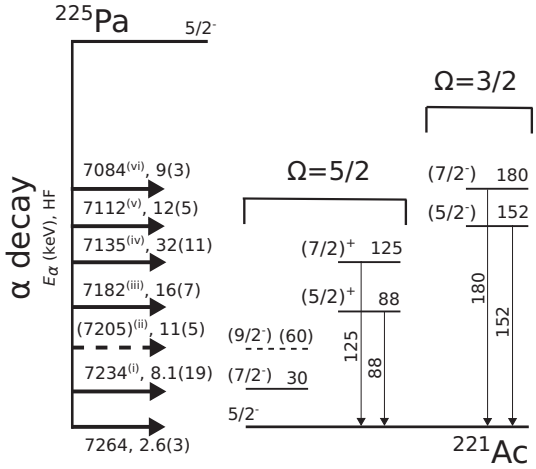

FIG. 5. Level scheme representing the ^{225}Pa $\rightarrow$ ^{221}Ac α decay. The details given are the same as in Fig. 4 with the additional indication of the Ω of the single-particle proton orbital to which the parity-doublet state is assigned. The α decays labeled (i)–(vi) correspond to those detailed in Table I and shown in Fig. 3.

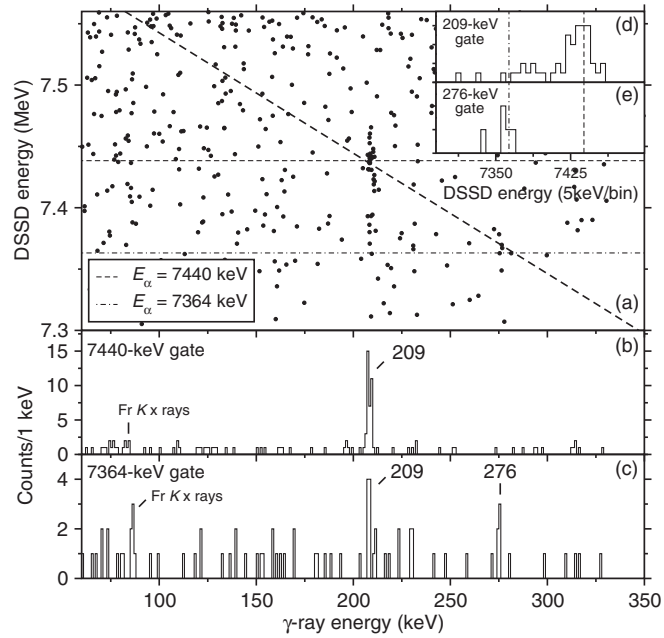

FIG. 6. Spectra from the $\alpha\gamma$-coincidence analysis of the decay of ^{221}Ac taken from Experiments 1 and 2. Panel (a) shows the energies of γ rays plotted against those of coincident α particles. Horizontal lines represent the energies of α particles from ^{221}Ac decays and the diagonal line represents the total Q value of the α decay of ^{221}Ac (Q_T = 7783 keV). The lower two panels give γ-ray energies in coincidence with 7440-keV α-particle energies (b) and 7364-keV α-particle energies, plus those with summed Auger electrons (c). Panels (d) and (e) show the α-particle energies measured in coincidence with 209- and 276-keV γ rays respectively.

directly to the ground state. Additionally, 209-keV γ rays are also observed, which implies a 67-keV transition between the 276- and 209-keV states. No 67-keV γ rays are observed in the $\alpha\gamma$-coincidence spectra, however this observation would not be expected considering the internal-conversion coefficients discussed below.

In order to understand the multipolarities of the three transitions established in ^{217}Fr several pieces of data were used. Only multipolarities with $\Delta I \leqslant 2$ are considered as the transitions were observed in prompt coincidence with α particles suggesting that higher-orders would be unlikely. In this context, a useful piece of data is the ratio between the intensities of α particles from decays populating excited states measured in the α-particle spectrum and those in coincidence with γ rays emitted from the populated excited states. This ratio is dependent on the total internal conversion coefficient of the γ-ray transition, which can be calculated as discussed in Ref. [29]; the measured intensity ratio may then be compared to those expected for different multipolarity assignments. For the 209-keV transition, the measured intensity ratio for the 7440-keV α particle is consistent only with an $E1$ or $E2$ assignment. It should also be noted that this comparison also rules out higher order multipolarity assignments.

The absence of 67-keV γ rays in coincidence with the 7364-keV α particles would suggest a large conversion coefficient for this transition, given that nine 209-keV γ rays are observed in coincidence with this α particle and the ratio of γ-ray efficiencies is $\epsilon_{209}/\epsilon_{67} \simeq 1.1$. This effectively precludes an $E1$ assignment for the 67-keV transition, as $\alpha_{\text{total}}(67_{E1}) = 0.29$ compared with $\alpha_{\text{total}}(67) \geqslant 8.5$ for all other multipolarities [29]. Figure 6(d) shows the α-particle energies measured in coincidence with the 209-keV γ ray; for the 7364-keV α particles this necessitates the subsequent decay via the 67-keV transition in question. The shifts in energy observed for the 7364-keV α particles by a few tens of keV is indicative of Auger-electron summing, which is discussed in more detail in Ref. [30] and illustrated in Fig. 2 therein. This, again, is a clear indication of a highly-converted 67-keV transition. Due to this energy summing the 7364-keV α-particle energy was determined from the coincidences with 276-keV γ rays, which are shown in Fig. 6(e). It should be noted that the 7364-keV α particles which sum with the conversion electrons from the 67-keV transition will be measured with energies around those of the 7440-keV α particles. These intensities were duly considered when calculating α-decay branching ratios.

The intensity of summed α particles with K conversion electrons, labeled as $\alpha + ce_K$ in Fig. 2(c), can also be used to help assign multipolarities for the transitions identified in ^{217}Fr. Using the measured intensities of the α particles from decays to excited states, the different $\alpha + ce_K$ intensities expected for all possible remaining combinations of multipolarities for the three transitions were simulated. Efficiencies for the total energy deposition from conversion electrons in the DSSD pixels were determined using Monte Carlo simulations. Values of around 37% were found for electron energies in the range of 50 to 300 keV, relevant to the present study. The possible multipolarity assignments consistent with the measured intensity of $\alpha + ce_K$ are determined to be 67($M1$ or $E2$), 209($E2$), and 276($M1$ or $E2$). Combinations of multipolarities which were inconsistent with parity changes in the established

level scheme were not considered. Neither were $M2$ multipolarity assignments for the 67-keV transition, which would be unlikely to compete with a lower-order multipolarity for the 276-keV transition.

Using the ^{217}Fr ground-state assignment of $I^\pi = 9/2^-$ taken from Refs. [11,15] the possible multipolarities established for the transitions then define the 209- and 276-keV states to have possible spins and parities: $I^\pi(209) = (5/2, 7/2, 9/2, 11/2, 13/2)^-$ and $I^\pi(276) = (5/2, 7/2, 9/2, 11/2, 13/2)^-$, with $\Delta I \leqslant 2$ between the two states. The branching ratios of the α decays from ^{221}Ac, and the branching ratio of the γ-ray transitions from the 276-keV state in ^{217}Fr, are calculated assuming $M1$ multipolarities for the 67- and 276-keV transitions; this is discussed in more detail in Sec. VI A.

B. ^{225}Pa → ^{221}Ac α decay

Figure 3(b) shows the spectrum from the α decay of ^{225}Pa selected using the conditions described in Sec. IV A 2. The α particles from decays identified to excited states are labeled $\alpha_{\text{(i)–(vi)}}$, corresponding to those listed in Table I and shown in Fig. 5. The α decay of ^{225}Pa produces a more complicated spectrum than that of ^{221}Ac, with α particles from multiple decays with closely spaced energies. This is presumably due to a higher density of low-energy states in the $N = 132$ daughter nucleus, ^{221}Ac, compared to those in the $N = 130$, transitional nucleus ^{217}Fr.

The 7264-keV α particle is assigned to the decay to the ground state of ^{221}Ac because this is the highest energy α particle, or α particle summed with an internal-conversion electron, in the decay of ^{225}Pa. The only other α particle which may be clearly identified from the spectrum in Fig. 3(b) is that with $E_\alpha = 7234$ keV.

In order to identify other α decays from ^{225}Pa, the spectrum of coincident γ-ray and α-particle energies shown in Fig. 3(c) was used. The total Q value for the α decay of ^{225}Pa, with $Q_T = 7395$ keV taken from the $E_\alpha = 7264$ keV of the decay which populates the ground state, is shown as a diagonal dashed line. Coincidences between fully detected α particles from ^{225}Pa decays which populate excited states in ^{221}Ac and γ rays from resulting transitions which directly populate the ground state from that excited state will appear on this line. Partially detected α-particle energies and Compton-scattered γ rays, along with α-particle energies measured in coincidence with γ rays emitted from cascades, will appear below this Q_T line.

Four $\alpha\gamma$ coincidences appear on the Q_T line, with $E_\gamma = 88$, 125, 152, and 180 keV. These coincidences are therefore assumed to indicate α decays which populate states with excitation energies equal to the energies of the γ rays. The four $\alpha\gamma$ coincidences correspond to α-particle energies indicated in Fig. 3(b) which are labeled (iii), (iv), (v), and (vi), respectively. More tentatively, one further α particle is identified from the spectrum in Fig. 3(b), which is labeled (ii) with $E_\alpha = 7205$ keV.

The 125-keV transition is further evident in the three counts observed in the projection of the γ-ray energies for all ^{225}Pa α-particle energies below 7264 keV, shown in Fig. 3(d). This then includes the ≈50% of α particles which escape from the surface of the DSSDs, depositing only a partial energy. Further understanding of the 125-keV transition may be gained by calculating the probabilities of observing three, or more, counts using total conversion coefficients, α_T, calculated for different multipolarity assignments [α_T(125 keV) = 0.29($E1$), 9.24($M1$), 4.12($E2$), 58.7($M2$) [29]]. These are found to be 0.42($E1$), 8.9×10^{-3}($M1$), 4.7×10^{-2}($E2$), 6.8×10^{-5}($M2$). These calculations use the α-particle intensities from decays which populate the 125-, 152-, and 180-keV states and assume that the 125-keV transition is passed through with 100% branching following the population of each of these states. Even with these conservative assumptions, as the probabilities are likely to be lower due to branching ratios in the level scheme, it is clear that all other multipolarities except $E1$ are unlikely for the 125-keV transition. The $E1$ assignment defines the I^π of the 125-keV state with $\Delta I \leqslant 1$ relative to that of the ground state, and with opposite parity. The multipolarity of the 88-keV transition is also assumed to be $E1$, with the same conclusions drawn for the 88-keV state, as the conversion coefficients for all other multipolarities are high: $\alpha_T = 0.16(E1)$, 5.0($M1$), 18.9($E2$), 95.1($M2$) [29].

When calculating the α-decay branching ratios from ^{225}Pa the I^π assignments discussed in Sec. VI B are assumed. Branching ratios of 100% are assumed for transitions between all populated states and the ground state, except for the 60-keV state which is assumed to populate only the level at 30 keV. Multipolarities of transitions from positive-parity states are assumed to be $E1$ and those from negative-parity states are assumed to be mixed $M1/E2$ with $\delta = 1$.

VI. DISCUSSION

Single-particle orbital energies from shell-model calculations can change rapidly with the addition of an octupole-deformation component to the quadrupole-deformed nuclear potential [4–6]. As this often leads to differences in the lowest-energy orbital, the experimentally determined ground-state spins and parities of odd-A nuclei may be compared with those expected from different calculations to indicate the presence, or not, of an octupole-deformation component. The nuclear chart in Fig. 7 shows part of the light-actinide region, with the odd-Z, even-N isotopes highlighted. The experimentally determined spin and parity assignments of the ground states are given as well as the Ω values of the orbitals populated by the odd protons for nuclei beyond the $N = 130$ transitional region. All information was taken from compilations and evaluations of nuclear data [25,31–37], and references therein. On the figure, boundary lines are given which define the region of odd-A nuclei in which the ground-state spins and parities are consistent with the lowest-lying orbitals calculated with the addition of an octupole deformation. Regions where data is not available, and the boundary is therefore uncertain, are indicated with dashed lines.

The figure has been adapted from Ref. [7] with several amendments, which are described below. Studies of the α decay of the even-Z, odd-N ^{227}U nucleus are consistent with a $I^\pi = 3/2^+$ assignment, which is expected for an $N = 135$

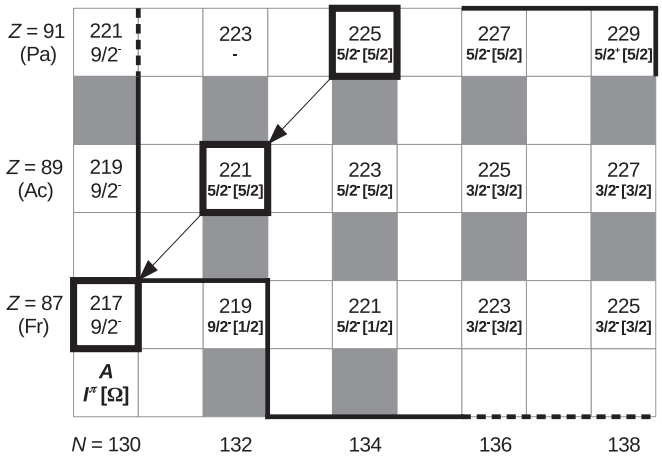

FIG. 7. Chart of nuclei for selected light actinides highlighting odd-Z even-N isotopes. Experimentally established ground-state spin and parity assignments are taken from Refs. [25,31–37] as well as the present work, and Ω values of the specific proton orbitals assigned to the ground-state configurations for isotopes beyond the $N = 130$ transitional region are given. The boundary lines define the region of odd-A nuclei in which the ground-state assignments are consistent with predictions from asymmetrically deformed nuclear-potential shell models; these are predominantly taken from Ref. [7], with additional amendments as described in the text. Additionally, the even-even nuclei which are predicted to possess ground-state octupole deformations in five, or more, of the calculations in Ref. [8] are shaded grey.

isotone in the asymmetrically deformed model [38,39]. This gives a reliable boundary at the top right of the figure. The boundary between At ($Z = 85$) and Rn ($Z = 86$) isotopes is confirmed at $N = 134$ due to the $I^\pi = 9/2^-$ (spherical shell model) ground-state assignment of ^{219}At [40]. The boundary is confirmed between $N = 130$ and 131 following α-decay studies of ^{219}Ra and ^{221}Th [30,41], as well as the present ground-state assignments, which are discussed below. More tentatively, this boundary is extended to the Pa isotopes as the ground state of ^{221}Pa has been assigned as $I^\pi = 9/2^-$ [42]. Additionally, the figure shows the even-even nuclei that are predicted to possess ground-state octupole deformations in five, or more, of the calculations in Ref. [8] as shaded grey.

A. Odd-*A* Ac ground-state configurations

Calculations of single-particle proton states in an asymmetrically-deformed nuclear potential consistently predict two orbitals, with $\Omega = 5/2$ and $\Omega = 3/2$, to be present at the Fermi level of the 89th proton of Ac isotopes from $N \approx 130$–140 [4–6]. The ground-state configurations of odd-A Ac isotopes are expected therefore, in the presence of strong octupole correlations, to be due to these orbitals, with the odd proton occupying the state lying lowest in energy. The calculations broadly predict that as both quadrupole- and octupole-deformation parameters decrease, from $N = 140$ down towards the spherical shell closure at $N = 126$, the $\Omega = 5/2$ and $3/2$ configurations cross, with the former becoming the lower-energy state.

The ground states of ^{227}Ac and ^{225}Ac have been assigned with $I^\pi = 3/2^-$. The assignment for ^{227}Ac was proposed following studies of the α decay of ^{231}Pa [43,44] and proton-stripping reactions [45] as well as direct measurements of the nuclear spin and electromagnetic moments, the latter helping to identify the single-particle orbital responsible for the ground-state configuration, via nuclear laser spectroscopy [46–49]. For ^{225}Ac, the assignment was made following studies of the α decay of ^{229}Pa [50,51] and the β^- decay of ^{225}Ra [51]. The ground state of ^{223}Ac was assigned as $I^\pi = 5/2^+$ following the study of the α decay of ^{227}Pa [52]. However, that interpretation was subsequently reevaluated following another α-decay study in Ref. [53], and the ground state was reassigned as $5/2^-$. These results were interpreted as the ground-state configurations switching from the $\Omega = 3/2$ (^{227}Ac and ^{225}Ac) to the $\Omega = 5/2$ (^{223}Ac) orbital between $N = 136$ and 134. For the next isotope, ^{221}Ac, a tentative $(3/2^-)$ ground-state was assigned following a study of prompt in-beam transitions by Aïche *et al.* in Ref. [9]. This assignment was guided by calculations of Ref. [6], which predict the energy of the $\Omega = 3/2$ orbital to be 8 keV below that of the $\Omega = 5/2$ orbital. However, these calculations also predicted the $\Omega = 5/2$-orbital energy to be 71 keV above that of the $\Omega = 3/2$ orbital in ^{223}Ac, contrary to experimental observations. The $3/2$ assignment in ^{221}Ac would imply that the $\Omega = 3/2$ and $5/2$ states cross again at $N = 132$, with the $3/2$ becoming the lowest in energy. For lower-N isotopes the ground states are determined by the odd proton occupying the $h_{9/2}$ spherical-shell-model orbital. This is evident in the $I^\pi = 9/2^-$ assignment for the ground state of ^{219}Ac from the observation of a dominant, unhindered α decay to the $9/2^-$ ground state of ^{215}Fr [11].

To interpret the present results from the ^{221}Ac $\rightarrow$ ^{217}Fr α decay, they may be compared with those from neighboring odd-A Ac isotopes. Figure 8(a) shows excitation energies of states in the isotopes ^{215}Fr, ^{217}Fr, ^{219}Fr, and ^{221}Fr populated in the α decay of ^{219}Ac [11,42], ^{221}Ac, ^{223}Ac [54,55], and ^{225}Ac [56,57], respectively. The configurations of states populated in ^{219}Fr and ^{221}Fr have previously been interpreted as members of parity-doublet bands built on two single-particle proton-orbital band heads with $\Omega = 1/2$ or $3/2$ [54–56]. Ground-state spins have also been directly determined and electromagnetic moments measured via laser spectroscopy in ^{219}Fr [58–60] and ^{221}Fr [59–64]. The study of the ground-state electric-quadrupole-moment systematics for odd-A francium isotopes (Ref. [59]) revealed ^{219}Fr and ^{221}Fr to possess similar deformations and confirmed the $\Omega = 1/2$ orbital assignment for both, despite the anomalous $I^\pi = 9/2^-$ ground state of ^{219}Fr. This is indicated by consistent electric-quadrupole-moment magnitudes from $^{219–225}$Fr, which change from negative to positive between ^{221}Fr and ^{223}Fr as the ground state changes between the $\Omega = 1/2$ and $3/2$ orbitals. This inversion is attributed to the strength of the Coriolis mixing; strong mixing decoupling the odd proton of the $\Omega = 1/2$ state in ^{219}Fr and ^{221}Fr and weaker mixing leading to a coupled $\Omega = 3/2$ proton for ^{223}Fr and ^{225}Fr. It should be noted that the $\Omega = 3/2$ states in Fr isotopes are the product of a different single-particle configuration to those discussed in the Ac isotopes. Ground-state assignments of $9/2^-$ are indicated for ^{215}Fr [11,65], ^{217}Fr

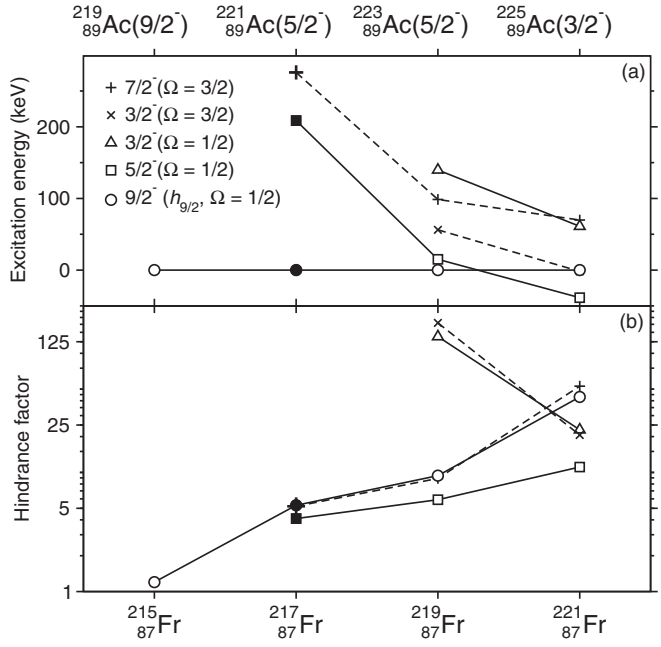

FIG. 8. Systematics of selected states in odd-A Fr isotopes (indicated on lower axis) showing excitation energies (a) and hindrance factors of α decays which populate the states (b). The decaying Ac isotope is shown on the upper axis, with the spin and parity assignment of the α-decaying state. The spins and parities of the states populated in Fr isotopes are indicated along with the Ω values of the reflection-asymmetric-potential model single-particle configurations; the spherical-shell-model configurations are also indicated where appropriate. Results are shown from the ^{219}Ac $\rightarrow$ ^{215}Fr [11,42], ^{223}Ac $\rightarrow$ ^{219}Fr [54,55], and ^{225}Ac $\rightarrow$ ^{221}Fr [56,57] α decays, as well as those for ^{221}Ac $\rightarrow$ ^{217}Fr from the present study, which are highlighted as filled or bold symbols.

[11], and ^{219}Fr [66,67], as a result of dominant, unhindered (HF $\simeq$ 1) α decays to $9/2^-$ $h_{9/2}$ spherical-shell-model ground states in the At ($Z = 85$) daughter nuclei. The presence of an unhindered decay from ^{219}Fr would indicate that this nucleus may be considered somewhat transitional; the $9/2^-$ ground state displaying characteristics of the $h_{9/2}$ spherical-shell-model configuration [7,55], as well as those of the $\Omega = 1/2$ orbital [59]. The $9/2^-$ states in Fig. 8 are therefore listed with both spherical-shell-model and reflection-asymmetric-model configurations, as the isotopes move from spherical (^{215}Fr), to transitional (^{217,219}Fr), and finally to the well-deformed region (^{221}Fr). It should be noted that the assignment of pure single-particle configurations to the states is somewhat misleading due to the significant Coriolis mixing expected. However, analogous states may still be identified in neighboring nuclei, the α-decay hindrance factors to which may be compared in interpreting the structures of the decaying states.

Figure 8(b) shows the hindrance factors of the α decays which populate the states shown in panel (a). The hindrance factors of the ^{225}Ac $\rightarrow$ ^{221}Fr and ^{223}Ac $\rightarrow$ ^{219}Fr α decays are consistent with the spin and parity assignments of the α-decaying ground states. Unhindered α decays from ^{225}Ac to the $3/2^-$ states in ^{221}Fr, and ^{223}Ac to the higher-spin $5/2^-$ and $7/2^-$ states in ^{219}Fr, are observed; decays to the $3/2^-$ states for ^{223}Ac $\rightarrow$ ^{219}Fr also become much more hindered. Clear shifts in hindrance factors to analogous states in the product nuclei are observed when changing the configuration of the α-decaying state from ^{225}Ac ($I^\pi = 3/2^-$) to ^{223}Ac ($I^\pi = 5/2^-$). For ^{221}Ac, the α decay to the $9/2^-$ ground state in ^{217}Fr shows no dramatic shift in hindrance factor compared to that of the ^{223}Ac decay to the $9/2^-$ ground state in ^{219}Fr. Such shifts in hindrance factor are observed between the α decays of (^{219}Ac and ^{223}Ac) and (^{223}Ac and ^{225}Ac) to $9/2^-$ ground states in the daughter nuclei, which is attributable to changes in configuration of the α-decaying state. This would suggest that the ground-state configuration in ^{221}Ac is the same as that in ^{223}Ac, that has a ground-state spin of 5/2.

Considering the configurations of the two excited states populated in ^{217}Fr following the α decay of ^{221}Ac, assignments of $I^\pi = 3/2^-$ for either state have been ruled out. This is evident from the observation of γ-ray transitions between the excited states in ^{217}Fr and the $9/2^-$ ground state; these transitions being unlikely to have $\Delta I \geqslant 3$ multipolarities (as detailed in Sec. V A). Considering the present suggestions for possible spins and parities of the 209- and 276-keV states in ^{217}Fr and the multipolarities of the three transitions identified from them, as well as the hindrance-factor systematics of neighboring isotopes, the two states are assigned as analogous to those with $I^\pi = (5/2)^-$ and $(7/2)^-$ of the $\Omega^\pi = 1/2^-$ and $3/2^-$ bands, respectively, in ^{219}Fr and ^{221}Fr. With decreasing quadrupole deformation when moving along the transitional nuclei from ^{219}Fr to ^{217}Fr the $9/2^-$ ground state is brought down in energy as a result of the spherical $h_{9/2}$ orbital. The excited $\Omega = 1/2$ and $3/2$ states therefore lie higher in energy for ^{217}Fr compared to ^{219}Fr. However, these states still remain below the excitation energies of states based on spherical-shell-model orbitals, for which the lowest energy is $E = 364$ keV [15].

The similarity of the α-decay fine structure from both ^{221}Ac and ^{223}Ac, and the difference to that of both ^{219}Ac and ^{225}Ac, is consistent with the same α-decaying state in both nuclei. The α-decaying ground state of ^{221}Ac is therefore assigned with $I^\pi = 5/2^-$, consistent with the assignment made for ^{223}Ac in Ref. [53], from the $\Omega = 5/2$ proton orbital. This assignment differs from that tentatively proposed in Ref. [9] of $I^\pi = (3/2^-)$, interpreted as from the $\Omega = 3/2$ state. The systematics of ground-state configurations in odd-A Ac nuclei, shown in Fig. 7, now indicates a crossing of the $\Omega = 3/2$ and 5/2 orbitals from $N = 136$ to 134, with the $\Omega = 5/2$ state becoming the lower in energy at $N = 134$, which persists to $N = 132$. This suggests that the asymmetrically deformed nuclear-potential model remains robust in calculating single-particle proton orbitals down to $N = 132$ for odd-A Ac isotopes, before the spherical-shell-model determines the $I^\pi = 9/2^-$ ground-state configurations at $N = 130$ and beyond down to the $N = 126$ shell closure.

B. Parity-doublet states in ^{221}Ac

The assigned spins and parities of the states populated in the ^{225}Pa $\rightarrow$ ^{221}Ac α decay are given in Table I, and shown in Fig. 5 with the Ω values of the single-particle orbitals indicated. Figure 9 compares the energies of the parity-doublet

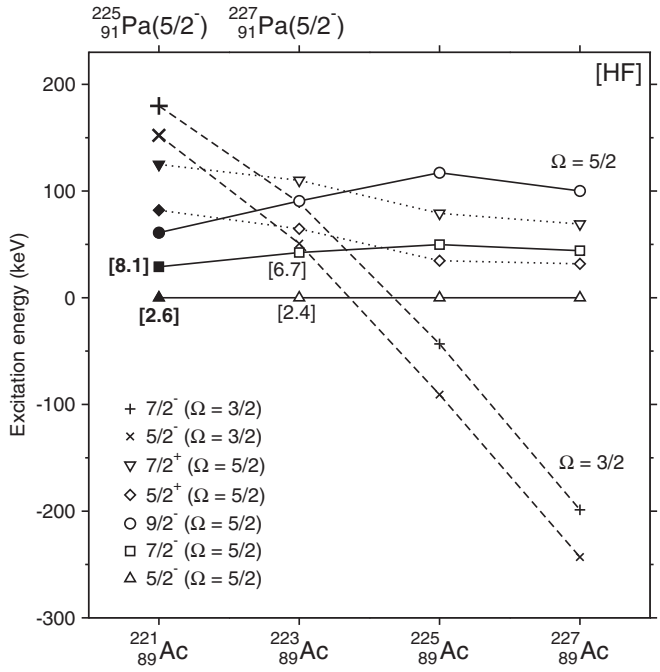

FIG. 9. Excitation-energy systematics in odd-A Ac isotopes (indicated on lower axis) of selected states from parity-doublet bands based on $\Omega = 5/2$ and $\Omega = 3/2$ single-particle proton orbitals shown relative to the $I^\pi = 5/2^-$ ($\Omega = 5/2$) state. Data are taken from Refs. [52,53] (^{223}Ac), [50,51] (^{225}Ac), and [43–45] (^{227}Ac), as well as present results for ^{221}Ac, which are highlighted with filled or bold symbols. Hindrance factors of α decays to some of the states are given in square brackets, with the preceding nucleus indicated on the upper axis with the spin and parity of the decaying state.

states identified in this work in ^{221}Ac with those in neighboring odd-A Ac isotopes from the $\Omega^\pi = 3/2^-$ and $\Omega^\pi = 5/2^\pm$ bands, taken from Refs. [52,53] (^{223}Ac), [50,51] (^{225}Ac), and [43–45] (^{227}Ac).

The ground state of ^{221}Ac populated in the α decay of ^{225}Pa has presently been assigned with $I^\pi = 5/2^-$, based on the $\Omega = 5/2$ orbital. In analogy to the states observed in ^{223,225,227}Ac, the state populated at 30 keV is assumed to be the $I^\pi = (7/2^-)$ member of the ground-state band. The unhindered α decays to these $(7/2^-)$ states in both ^{221}Ac and ^{223}Ac suggests a $I^\pi = 5/2^-(\Omega = 5/2)$ ground-state assignment of ^{225}Pa; this is discussed in more detail in Sec. VI C. Other states populated in the $\Omega^\pi = 5/2^\pm$ bands are assigned according to systematics of excited states and α-decay hindrance factors to the states, as well as the established spin and parity information for the 88- and 125-keV states, as detailed in Sec. V B.

In addition to states in ^{221}Ac in the ground-state $\Omega = 5/2$ band, those in the $\Omega = 3/2$ band are also expected to be populated via α decay. In both cases it is the states with similar spins and parities to those of the α-decaying ^{225}Pa ground state that are expected to be populated via unhindered decays. From the α decays identified, the transitions with $E_\alpha = 7112$ and 7084 keV would likely correspond to decays which populate states in the $\Omega = 3/2$ band. Tentative assignments have been made for two states populated in this band based on excitation-energy and hindrance-factor systematics. It is possible that the 152-keV state could be assigned as the $(3/2^-)$ state of the $\Omega = 3/2$ band, with the 180-keV state then being the $(5/2^-)$ state. However, due mainly to the hindrance-factor systematics the 152- and 180-keV states are assigned as the $(5/2^-)$ and $(7/2^-)$ members of the $\Omega = 3/2$ band, respectively.

The systematics given in Fig. 9 show the $I^\pi = 9/2^-$ member of the $\Omega = 5/2$ orbital band continues to move down in energy at $N = 132$. This precedes the dramatic shift observed in the $N = 130$ transitional nucleus ^{219}Ac, in which the $I^\pi = 9/2^-$ state becomes the ground state based on the $h_{9/2}$ spherical-shell-model orbital [11]. The $\pm\pi$ parity-doublet partner states are observed to deviate in energy when moving from the center of the region of quadrupole-octupole deformation ($N \approx 136$). However, no dramatic change in energy difference is observed moving down to ^{221}Ac, suggesting that octupole correlations remain strong to the edge of the region. The present results suggest that the $\Omega = 3/2$ bandhead lies around 120 keV above that of the $\Omega = 5/2$ orbital in ^{221}Ac. This is consistent with various calculations of single-particle orbital energies in the presence of asymmetrically deformed nuclear potentials [4–6], suggesting the model remains robust down to $N = 132$ for the Ac isotopes.

C. Odd-*A* Pa ground-state configurations

As in the odd-A Ac isotopes, the $\Omega = 3/2$ and $\Omega = 5/2$ proton orbitals are expected to determine the ground-state configurations of the odd-A Pa isotopes in the region of strong octupole correlations [4–6]. However, it is now the higher-energy orbital, occupied by the 91st proton of the Pa isotopes, as opposed to the lower-energy orbital, occupied by the 89th proton of Ac, which determines the ground-state configuration. The crossing of the $\Omega = 3/2$ and 5/2 orbitals, predicted to occur with the change in quadrupole deformation and observed in the Ac isotopes from $N = 136$ to 134, is therefore expected to lead to the opposite shift in ground-state configurations than that observed in the odd-A Ac isotopes; from $\Omega = 5/2$ to $\Omega = 3/2$ configurations when moving down towards the $N = 126$ shell closure.

The ground states of ^{229}Pa and ^{227}Pa have been assigned to be $I^\pi = 5/2^+$ and $5/2^-$, respectively, and attributed to the $\Omega = 5/2$ orbital. The assignments were made for ^{229}Pa following electron-capture studies to, and from, the isotope, as well as multinucleon transfer reactions and α-decay studies [51,68,69] and for ^{227}Pa following α-decay studies to states in ^{223}Ac [52,53]. No assignments for the ground states of ^{225}Pa or ^{223}Pa have previously been proposed. The unhindered, dominant α decay from ^{221}Pa to the $I^\pi = 9/2^-$ spherical-shell-model ground state of ^{217}Ac [42] leads to the same $9/2^-$ assignment for the decaying ground state.

Figure 9 indicates the hindrance factors of α decays to some of the states populated in odd-A Ac isotopes, taken from Refs. [52,53] (^{227}Pa $\rightarrow$ ^{223}Ac) and the present study (^{225}Pa $\rightarrow$ ^{221}Ac). The ^{227}Pa $\rightarrow$ ^{223}Ac α decay has been noted for being somewhat unusual in the decay of an odd-A nucleus as having the same initial and final state configurations for the ground-state-to-ground-state α decay [53]; the inversion of the $\Omega = 3/2$ and $\Omega = 5/2$ orbitals between ^{225}Ac and

^{223}Ac leads to both the mother and daughter nuclei having $I^\pi = 5/2^-$ ($\Omega = 5/2$) ground states. This leads to an unhindered decay to the ground state (HF = 2.4), and also the $I^\pi = 7/2^-$ member of the band (HF = 6.7), with $\Delta I = 1$ required. The low hindrance factors to the $5/2^-$ (HF = 2.6) and $(7/2^-)$ (HF = 8.1) members of the $\Omega = 5/2$ band in ^{221}Ac identified in this work would imply the same situation with the ^{225}Pa → ^{221}Ac decay, leading to the $I^\pi = 5/2^-$ ($\Omega = 5/2$) ground-state assignment for ^{225}Pa. An $I^\pi = 3/2^-$ ($\Omega = 3/2$) assignment for the α-decaying state would be inconsistent with the low hindrance factors observed. Relatively unhindered α decays to states in the $\Omega = 3/2$ band are also observed from both ^{227}Pa and ^{225}Pa, with hindrance factors of 4.8 (^{227}Pa) and 12 (^{225}Pa) to the respective $(5/2^-)$ states. However, uncertainties in branching ratios to, and spin and parity assignments for, states in the $\Omega = 3/2$ bands of ^{223}Ac and ^{221}Ac make comparison difficult. Hindrance factors to the positive-parity states in ^{223}Ac and ^{221}Ac are also difficult to compare due to the varying strength of octupole correlations across the region and the effects this has on initial- and final-state wave-function overlap in the α decays.

The $I^\pi = 5/2^-$ ($\Omega = 5/2$) ground-state assignment for ^{225}Pa indicates that the crossing of the $\Omega = 3/2$ and $\Omega = 5/2$ orbitals, which occurs between $N = 136$ (^{225}Ac) and 134 (^{223}Ac) for the Ac isotopes, does not occur by $N = 134$ in the Pa isotope chain. As the crossing of the orbitals is predicted to take place with reducing quadrupole deformation [4–6] this is unsurprising, as the predicted deformation parameters are calculated to be $\beta_2 = 0.164$ for ^{225}Ac, where the orbital crossing has not yet occurred in the Ac isotopes, and $\beta_2 = 0.165$ for ^{225}Pa [70]. Considering the next isotope, ^{223}Pa, the orbitals may be expected to have crossed, meaning the $\Omega = 3/2$ orbital will form the ground state. This expectation is due to the calculated quadrupole-deformation parameter of $\beta_2 = 0.137$ for ^{223}Pa, compared with $\beta_2 = 0.147$ for ^{223}Ac in which the orbitals are observed to have crossed. However, the predicted $\Omega = 3/2$-orbital ground state assumes that the picture of quadrupole-octupole deformed nuclear systems is still valid for ^{223}Pa.

VII. SUMMARY

Low-lying states in the odd-Z, even-N nuclei ^{221}Ac and ^{225}Pa have been investigated by means of the α-particle, conversion-electron, and γ-ray spectroscopy of the ^{225}Pa → ^{221}Ac → ^{217}Fr decay chain. Ground-state assignments of $I^\pi = 5/2^-$ have been made for both ^{221}Ac and ^{225}Pa, which were attributed to the odd proton occupying the asymmetrically deformed nuclear-potential orbital with $\Omega = 5/2$. The odd proton inhabits this state in both Ac (89th) and Pa (91st) isotopes due to the crossing of the $\Omega = 5/2$ and $3/2$ orbitals in the region. Parity-doublet states populated in ^{221}Ac above the $\Omega = 5/2$ and $3/2$ bandheads were also assigned. These results indicate that an asymmetrically deformed nuclear ground state persists in the odd-A isotopes down to $N = 132$ for Ac and $N = 134$ for Pa. This is proposed as the single-particle states predicted by the asymmetrically deformed nuclear-potential shell model remain valid, and is supported, in the Ac isotopes, by the observation of possible parity-doublet states.

ACKNOWLEDGMENTS

This work is supported in part by the following bodies: STFC (UK) under Grants No. ST/L005808/1 and No. ST/P005101/1 (UWS); the EU 7th Framework Programme, Integrating Activities Transnational Access, Project No. 262010 (ENSAR); the Academy of Finland under the Finnish Centre of Excellence Programme (Nuclear and Accelerator Based Physics Programme at JYFL); the Scottish Universities Physics Alliance, Glasgow, United Kingdom (SUPA); the Slovak Research and Development Agency under Contract No. APVV-20-0532; the Slovak grant agency VEGA (Contract No. 2/0067/21); and the project ITMS code 26210120023, supported by the Research and Development Operational Programme funded by ERDF. The authors would also like to acknowledge GAMMAPOOL support for the JUROGAM HPGe detectors.

[1] I. Ahmad and P. A. Butler, Annu. Rev. Nucl. Part. Sci. **43**, 71 (1993).
[2] P. A. Butler and W. Nazarewicz, Rev. Mod. Phys. **68**, 349 (1996).
[3] P. A. Butler, J. Phys. G: Nucl. Part. Phys. **43**, 073002 (2016).
[4] G. A. Leander and R. K. Sheline, Nucl. Phys. A **413**, 375 (1984).
[5] G. A. Leander and Y. S. Chen, Phys. Rev. C **37**, 2744 (1988).
[6] S. Ćwiok and W. Nazarewicz, Nucl. Phys. A **529**, 95 (1991).
[7] R. K. Sheline, Phys. Lett. B **197**, 500 (1987).
[8] Y. Cao, S. E. Agbemava, A. V. Afanasjev, W. Nazarewicz, and E. Olsen, Phys. Rev. C **102**, 024311 (2020).
[9] M. Aïche, M. Bentaleb, Ch. Briançon, A. Chevallier, J. Chevallier, J. S. Dionisio, J. Fernández Niello, R. Kulessa, E. Lubkiewicz, J. S. Dionisio *et al.*, Nucl. Phys. A **567**, 685 (1994).
[10] R. L. Hahn, M. F. Roche, and K. S. Toth, Nucl. Phys. A **113**, 206 (1968).
[11] J. Borggreen, K. Valli, and E. K. Hyde, Phys. Rev. C **2**, 1841 (1970).
[12] M. Huyse, P. Dendoovena, and K. Deneffe, Nucl. Instrum. Methods Phys. Res., Sect. B **31**, 483 (1988).
[13] A. N. Andreyev, D. D. Bogdanov, V. I. Chepigin, M. Florek, A. P. Kabachenko, O. N. Malyshev, S. Saro, G. M. Ter-Akopian, M. Veselsky, and A. V. Yeremin, Joint Institute for Nuclear Research Report No. JINR-E7-92-279, 1992 (unpublished).
[14] A. K. Mistry, Z. Zhang, F. P. Heßberger, D. Ackermann, B. Andel, S. Antalic, M. Block, P. Chhetri, F. Dechery, C. Droese *et al.*, Acta Phys. Pol. B **49**, 613 (2018).
[15] M. Aïche, A. Chevallier, J. Chevallier, S. Hulne, S. Khazrouni, N. Schulz, and J. C. Sens, J. Phys. G **14**, 1191 (1988).
[16] M. Sakama, K. Tsukada, M. Asai, S. Ichikawa, H. Haba, S. Goto, Y. Oura, I. Nishinaka, Y. Nagame, M. Shibata *et al.*, Eur. Phys. J. A **9**, 303 (2000).

[17] E. Parr, J. F. Smith, P. T. Greenlees, K. Auranen, P. A. Butler, R. Chapman, D. M. Cox, D. M. Cullen, L. P. Gaffney, T. Grahn *et al.*, Phys. Rev. C **100**, 044323 (2019).

[18] J. Pakarinen, P. Papadakis, J. Sorri, R.-D. Herzberg, P. T. Greenlees, P. A. Butler, P. J. Coleman-Smith, D. M. Cox, J. R. Cresswell, P. Jones *et al.*, Eur. Phys. J. A **50**, 53 (2014).

[19] M. Leino, Nucl. Instrum. Methods Phys. Res., Sect. B **126**, 320 (1997).

[20] J. Uusitalo, P. Jones, P. Greenlees, P. Rahkila, M. Leino, A. N. Andreyev, P. A. Butler, T. Enqvist, K. Eskola, T. Grahn *et al.*, Nucl. Instrum. Methods Phys. Res., Sect. B **204**, 638 (2003).

[21] R. D. Page, A. N. Andreyev, D. E. Appelbe, P. A. Butler, S. J. Freeman, P. T. Greenlees, R.-D. Herzberg, D. G. Jenkins, G. D. Jones, P. Jones *et al.*, Nucl. Instrum. Methods Phys. Res., Sect. B **204**, 634 (2003).

[22] I. H. Lazarus, D. E. Appelbe, P. A. Butler, P. J. Coleman-Smith, J. R. Cresswell, S. J. Freeman, R.-D. Herzberg, I. Hibbert, D. T. Joss, S. C. Letts *et al.*, IEEE Trans. Nucl. Sci. **48**, 567 (2001).

[23] P. Rahkila, Nucl. Instrum. Methods Phys. Res., Sect. A **595**, 637 (2008).

[24] W. J. Huang, Meng Wang, F. G. Kondev, G. Audi, and S. Naimi, Chin. Phys. C **45**, 030002 (2021).

[25] F. G. Kondev, E. A. McCutchan, B. Singh, K. Banerjee, S. Bhattacharya, A. Chakraborty, S. Garg, N. Jovancevic, S. Kumar, S. K. Rathi *et al.*, Nucl. Data Sheets **147**, 382 (2018).

[26] M. S. Basunia, Nucl. Data Sheets **108**, 633 (2007).

[27] J. Chen and F. G. Kondev, Nucl. Data Sheets **126**, 373 (2015).

[28] M. A. Preston, Phys. Rev. **71**, 865 (1947).

[29] T. Kibédi, T. W. Burrows, M. B. Trzhaskovskaya, P. M. Davidson, and C. W. Nestor, Nucl. Instrum. Methods Phys. Res., Sect. A **589**, 202 (2008).

[30] E. Parr, J. F. Smith, P. T. Greenlees, K. Auranen, R. Chapman, D. M. Cullen, T. Grahn, L. Grocutt, A. Herzáň, R.-D. Herzberg *et al.*, Phys. Rev. C **102**, 054335 (2020).

[31] F. G. Kondev, M. Wang, W. J. Huang, S. Naimi, and G. Audi, Chin. Phys. C **45**, 030001 (2021).

[32] B. Singh, G. Mukherjee, S. K. Basu, S. Bhattacharya, S. Bhattacharya, A. Chakraborti, A. K. De, R. Gowrishankar, A. K. Jain, S. Kumar, and S. Singh, Nucl. Data Sheets **175**, 150 (2021).

[33] A. K. Jain, S. Singh, S. Kumar, and J. K. Tuli, Nucl. Data Sheets **108**, 883 (2007).

[34] E. Browne, Nucl. Data Sheets **93**, 763 (2001).

[35] A. K. Jain, R. Raut, and J. K. Tuli, Nucl. Data Sheets **110**, 1409 (2009).

[36] F. Kondev, E. McCutchan, B. Singh, and J. Tuli, Nucl. Data Sheets **132**, 257 (2016).

[37] E. Browne and J. K. Tuli, Nucl. Data Sheets **109**, 2657 (2008).

[38] T. H. Hoare, P. A. Butler, G. D. Jones, M. Loiselet, O. Naviliat-Cuncic, J. Vervier, M. Dahlinger, A. M. Y. El-Lawindy, R. Wadsworth, and D. L. Watson, J. Phys. G **17**, 145 (1991).

[39] Z. Kalaninová, S. Antalic, F. P. Heßberger, D. Ackermann, B. Andel, B. Kindler, M. Laatiaoui, B. Lommel, and J. Maurer, Phys. Rev. C **92**, 014321 (2015).

[40] A. E. Barzakh, J. G. Cubiss, A. N. Andreyev, M. D. Seliverstov, B. Andel, S. Antalic, P. Ascher, D. Atanasov, and D. Beck, Phys. Rev. C **99**, 054317 (2019).

[41] R. K. Sheline, C. F. Liang, P. Paris, A. Gizon, and V. Barci, Phys. Rev. C **49**, 725 (1994).

[42] H. Miyatake, T. Nomura, S. Kubono, J. Tanaka, M. Oyaizu, H. Okawa, N. Ikeda, K. Sueki, H. Kudo *et al.*, Nucl. Phys. A **501**, 557 (1989).

[43] W. Teoh, R. D. Connor, and R. H. Betts, Nucl. Phys. A **319**, 122 (1979).

[44] I. Aničin, I. Bikit, C. Girit, H. Güven, W. D. Hamilton, and A. A. Yousif, J. Phys. G **8**, 369 (1982).

[45] H. E. Martz, R. K. Sheline, R. G. Lanier, R. W. Hoff, G. L. Struble, D. J. Decman, D. G. Burke, R. R. Chasman, and R. A. Naumann, Phys. Rev. C **37**, 1407 (1988).

[46] F. S. Tomkins, M. Fred, and W. F. Meggers, Phys. Rev. **84**, 168 (1951).

[47] M. Fred, F. S. Tomkins, and W. F. Meggers, Phys. Rev. **98**, 1514 (1955).

[48] R. Ferrer, A. Barzakh, B. Bastin, R. Beerwerth, M. Block, P. Creemers, H. Grawe, R. de Groote, P. Delahaye, X. Fléchard *et al.*, Nat. Commun. **8**, 14520 (2017).

[49] C. Granados, P. Creemers, R. Ferrer, L. P. Gaffney, W. Gins, R. de Groote, M. Huyse, Yu. Kudryavtsev, Y. Martínez, S. Raeder *et al.*, Phys. Rev. C **96**, 054331 (2017).

[50] P. Aguer, A. Peghaire, and C. F. Liang, Nucl. Phys. A **202**, 37 (1973).

[51] I. Ahmad, J. E. Gindler, A. M. Friedman, R. R. Chasman, and T. Ishii, Nucl. Phys. A **472**, 285 (1987).

[52] I. Ahmad, R. Holzmann, R. V. F. Janssens, P. Dendooven, M. Huyse, G. Reusen, J. Wauters, and P. Van Duppen, Nucl. Phys. A **505**, 257 (1989).

[53] R. K. Sheline, C. F. Liang, and P. Paris, Int. J. Mod. Phys. A **5**, 2821 (1990).

[54] C. F. Liang, P. Paris, and R. K. Sheline, Nucl. Phys. A **520**, c361 (1990).

[55] C. F. Liang, P. Paris, J. Kvasil, and R. K. Sheline, Phys. Rev. C **44**, 676 (1991).

[56] G. Ardisson, J. Gasparro, V. Barci, and R. K. Sheline, Phys. Rev. C **62**, 064306 (2000).

[57] S. A. Kudrya, V. M. Gorozhankin, K. Ya. Gromov, Sh. R. Malikov, L. A. Malov, V. A. Sergienko, V. I. Fominyka, V. V. Tsupko-Sitnikov, V. G. Chumin, and E. A. Yakushev, Joint Institute for Nuclear Research Report No. JINR-E6-2002-202, 2002 (unpublished).

[58] I. Budinčević, J. Billowes, M. L. Bissel, T. E. Cocolios, R. P. de Groote, S. De Schepper, V. N. Fedosseev, K. T. Flanagan, S. Franchoo, R. F. Garcia Ruiz *et al.*, Phys. Rev. C **90**, 014317 (2014).

[59] R. P. de Groote, I. Budinčević, J. Billowes, M. L. Bissel, T. E. Cocolios, G. J. Farooq-Smith, V. N. Fedosseev, K. T. Flanagan, S. Franchoo, R. F. Garcia Ruiz *et al.*, Phys. Rev. Lett. **115**, 132501 (2015).

[60] A. E. Barzakh, D. Atanasov, A. N. Andreyev, M. Al Monthery, N. A. Althubiti, B. Andel, S. Antalic, K. Blaum, T. E. Cocolios, J. G. Cubiss *et al.*, Phys. Rev. C **101**, 064321 (2020).

[61] C. Ekström, S. Ingelman, G. Wannberg, and M. Skarestad, Phys. Scr. **18**, 51 (1978).

[62] A. Coc, C. Thibault, F. Touchard, H. T. Duong, P. Juncar, S. Liberman, J. Pinard, J. Lermé, J. L. Vialle, S. Büttgenbach *et al.*, Phys. Lett. B **163**, 66 (1985).

[63] A. Coc, C. Thibault, F. Touchard, H. T. Duong, P. Juncar, S. Liberman, J. Pinard, M. Carre, J. Lermé, J. L. Vialle *et al.*, Nucl. Phys. A **468**, 1 (1987).

[64] K. M. Lynch, J. Billowes, M. L. Bissell, I. Budinčević, T. E. Cocolios, R. P. De Groote, S. De Schepper, V. N. Fedosseev, K. T. Flanagan, S. Franchoo *et al.*, Phys. Rev. X **4**, 011055 (2014).

[65] T. Nomura, K. Hiruta, M. Yoshie, and O. Hashimoto, Phys. Rev. C **9**, 1168 (1974).

[66] G. Graeffe and P. Kauranen, J. Inorg. Nucl. Chem. **28**, 933 (1966).

[67] C. F. Liang, P. Paris, and R. K. Sheline, Phys. Rev. C **47**, 1801 (1993).

[68] I. Ahmad, J. E. Gindler, R. R. Betts, R. R. Chasman, and A. M. Friedman, Phys. Rev. Lett. **49**, 1758 (1982).

[69] I. Ahmad, R. R. Chasman, J. P. Greene, F. G. Kondev, and S. Zhu, Phys. Rev. C **92**, 024313 (2015).

[70] P. Möller, J. R. Nix, W. D. Myers, and W. J. Swiatecki, At. Data Nucl. Data Tables **59**, 185 (1995).